Carbohydrate Polymers 90 (2012) 462–471

Contents lists available at SciVerse ScienceDirect

Carbohydrate Polymers

journal homepage: www.elsevier.com/locate/carbpol

Preparation and optimization of surface-treated methotrexate-loaded nanogels intended for brain delivery

Amir Azadi[a], Mehrdad Hamidi[b], Mohammad-Reza Khoshayand[c], Mohsen Amini[d], Mohammad-Reza Rouini[a,*]

[a] Biopharmaceutics and Pharmacokinetic Division, Department of Pharmaceutics, Faculty of Pharmacy, Tehran University of Medical Sciences, P.O. Box 14155-6451, Tehran, Iran
[b] Department of Pharmaceutics, School of Pharmacy, Zanjan University of Medical Sciences, P.O. Box 45139-56184, Zanjan, Iran
[c] Department of Drug and Food Control, Faculty of Pharmacy, Tehran University of Medical Sciences, P.O. Box 14155-6451, Tehran, Iran
[d] Department of Medicinal Chemistry and Drug Design and Development Research Centre, Faculty of Pharmacy, Tehran University of Medical Sciences, P.O. Box 14155-6451, Tehran, Iran

ARTICLE INFO

Article history:
Received 29 February 2012
Received in revised form 21 April 2012
Accepted 20 May 2012
Available online 30 May 2012

Keywords:
Hydrogel nanoparticles
Multi-objective optimization
Surface functionalization
Chitosan
Methotrexate
Polysorbate 80

ABSTRACT

Nanogels loaded with methotrexate (MTX) were prepared via an ionic gelation process using chitosan and sodium tripolyphosphate (TPP). The preparation process was optimized by a systematic multi-objective-optimization approach in terms of the size, poly-dispersity index (PDI), loading efficiency (LE) and loading capacity (LC) of the resulting nanocarriers. A combination of the pH of the chitosan solution, the addition time of the TPP solution and temperature effects accounted for nearly 75% of the variation in nanogel size; the TPP initial concentration had a very significant effect on LE ($p < 0.0001$). The final particle size (*Z*-average (*r* nm)), PDI, LE and LC corresponding to the optimal conditions were 59.27 nm, 0.34, 61.82% and 53.68%, respectively. As the ultimate goal, the surfaces of the MTX-loaded nanogels were modified by polysorbate 80 for the purpose of brain targeting. The cumulative in vitro release profiles of surfactant-coated and uncoated nanogels were almost identical and showed acceptable performance.

1. Introduction

Hydrogel nanoparticles (generally referred to as nanogels) have attracted a great deal of interest in the field of nanotechnology-based drug delivery owing to their unique potential resulting from combining the properties of a hydrogel system (e.g., hydrophilicity and extremely high water absorptivity) with a nanoparticulate system (e.g., very small size). Among the polymers used for nanogel fabrication, chitosan is the most widely used. This commercially and academically interesting biopolymer is a biodegradable polysaccharide made of 2-amino-2-deoxy-D-glucose monomers with high desirability for human applications (Hamidi, Azadi, & Rafiei, 2008; Hamidi, Azadi, Mohamadi-Samani, Rafiei, & Ashrafi, 2012; Yuan, Shah, Hein, & Misra, 2010). Methotrexate (MTX) is a widely used chemotherapeutic agent with a prominent position in the treatment of different cancers and autoimmune diseases (Case, 2001; Hitchings & Elion, 1963; Kratz, Abu Ajaj, & Warnecke, 2007). Methotrexate inhibits dihydrofulate reductase (DHFR), an enzyme that competitively participates in tetrahydrofulate synthesis. Therefore, it can interfere in the synthesis of DNA, RNA and proteins. Central nervous system (CNS) malignancies are rare but extremely life-threatening cancers suffering from limited drug access to the tumor site because of the blood–brain barrier (BBB), a specialized barrier located at brain capillary endothelial cells with the purpose of controlling the passage of different harmful xenobiotics into the brain parenchyma (Stein, Kuten, Ben-Arieh, Cohen, & Haim, 1991). Fortunately, the implementation of MTX-based chemotherapy has improved survival rates for this patient population; however, a major defect in this context is poor drug permeability through the BBB (Abrey, Yahalom, & DeAngelis, 2000; Hochberg, Loeffler, & Prados, 1991; Ng, Rosenthal, Ashley, & Cher, 2000). The BBB is a physical as well as biochemical barrier comprised of the endothelial cells of brain capillaries equipped with tight junctions between neighboring cells, thereby limiting the entry of substances via the paracellular route into the brain parenchyma. Furthermore, there exists a complex and efficient biochemical orchestra within the BBB consisting of, mainly, different transporters and enzymes working together to keep the vital CNS organs protected from different harmful chemicals and xenobiotics and to maintain CNS homeostasis. In fact, the extensive and continuous tight junctions that exist between cerebral capillary endothelial cells significantly restrict the transport of

* Corresponding author. Tel.: +98 21 66959056; fax: +98 21 66959056.
E-mail address: rouini@tums.ac.ir (M.-R. Rouini).

0144-8617/$ – see front matter © 2012 Elsevier Ltd. All rights reserved.
http://dx.doi.org/10.1016/j.carbpol.2012.05.066

many substances from the bloodstream to the CNS via the paracellular pathway (Koziara, Lockman, Allen, & Mumper, 2006). At the membrane of these specialized cells are found several ATP-binding cassette (ABC) transporters, e.g. P-glycoprotein (P-gp), multidrug resistance-associated proteins (MRP) and ABCG2, which pump transported substances back into the blood circulation (Koziara et al., 2006; Linnet and Ejsing, 2008). Several studies have attempted to overcome the BBB to facilitate CNS entry of CNS-active therapeutic agents, mainly by promoting osmotic opening of tight junctions (Greig, 1992), as well as designing pro-drugs or using carrier systems such as various nanoparticles (Huwyler, Wu, & Pardridge, 1996; Koziara et al., 2006). Among these, polymeric nanoparticles are promising candidates because some of these carriers have great potential to pass through the tight junctions of the BBB, and others may mask the drug from being detected by the enzymes or transporters (Wang et al., 2010). It has been demonstrated that nanoparticles made from hydrophilic polymers such as chitosan with a particle size less than 100 nm can evade clearance from the blood circulation by the reticuloendothelial system (RES) (Wilson et al., 2010). In this context, the surface functionalization of polymeric nanoparticles can also play an important role in CNS influx of these nanocarriers. The main strategy in this functionalization is based on targeting various biomolecules expressed at the BBB (Wong, Chattopadhyay, Wu, & Bendayan, 2010). Low-density lipoprotein (LDL) receptor targeting has been exploited as one of the most effective ways to improve drug brain entry in a specific manner. LDL receptor targeting can be achieved efficiently by coating nanoparticles with polysorbate. Studies have revealed that polysorbate (especially polysorbate 80) can induce apolipoprotein E (apoE) adsorption onto the nanoparticle surface, and these apoE-enriched nanoparticles probably proceed via the LDL receptor-mediated endocytic pathway at brain endothelial cells (Gulyaev et al., 1999; Olivier et al., 1999).

The classical method of nanogels preparation optimization based on changing one parameter at a time while keeping the others at fixed levels is laborious and time consuming. This method requires a complete series of experiments for every factor of interest. Moreover, such a method does not provide means of observing possible factor interactions. In contrast, factorial experimental designs offer a number of important advantages. For instance, the researcher could easily determine factor effects with considerably less experimental effort, identify factors, find optima, offer greater precision (Leiro, Siso, Ortega, Santamarina, & Sanmartin, 1995) and facilitate system modeling (Miron, Siso, Murado, & Gonzalez, 1988). Identification of the experimental conditions which result in the best responses is the main goal in optimization studies. However, dependent variables may sometimes be contradictory and require optimal compromises to be determined between them. It means that obtaining an optimal procedure requires different dependent and independent variables to be simultaneously set. To overcome this problem, in a process known as multi-objective optimization (MOO), desirability functions are used (Deming, 1991). This approach was first introduced by Derringer and Suich (1980). In this study, the primary objective was to screen the factors affecting the preparation of MTX-loaded nanogels and then to explore the optimum conditions for obtaining nanogels with a high drug payload while maintaining small particle size using statistical response surface methodology. The ultimate aim of this step was to present a novel and comprehensive approach for multi-objective optimizing the nanogel preparation. Thereafter, nanogels surface functionalized with polysorbate 80 were fabricated to ultimately improve brain drug delivery. Finally, a series of in vitro characterization tests were carried out on the prepared functionalized nanogels to evaluate their potential for entry prior to our prospective final step of in vivo investigations in animal models. The results of this study will help us to neuropharmacokinetic modeling and evaluation of MTX-loaded nanogels in animal models as a conclusive goal and one of the novel aspects of our project which was not reported until now.

2. Materials and methods

2.1. Materials

Chitosan (degree of deacetylation up to 90% with viscosity values of 6 and 463 cp) was purchased from Perimex (Iceland, Art. no. TM 3142 and TM 3425). Pentasodium triphosphate (TPP; Merck, Germany, Lot no. K36643499-742) was purchased locally. Methotrexate was kindly donated by Loghman Pharmaceutical Co. (Tehran, Iran). All other chemicals, solvents and reagents used were chemical or analytical grade, as needed, and were purchased locally.

2.2. Experimental design

A systematic multi-objective optimization approach was used throughout the present study for optimization of the nanogel preparation method in terms of the final *Z*-average of the particle size, poly-dispersity index, loading efficiency and loading capacity of the resulting nanoparticles. The method consisted of two steps, including screening and optimization.

2.2.1. Screening

A Plackett Burman design was performed to determine factors with a significant effect on nanogel size and drug loading efficiency. The pH of the chitosan solution, temperature, TPP initial concentration, addition time of the TPP solution and the rate of stirring were the numeric factors, and chitosan molecular weight was the categorical factor considered important based on the preliminary tests. All experiments were carried out in triplicate. The factors involved in the study with the corresponding levels are shown in Table 1.

2.2.2. Optimization

A D-optimal design was planned to determine the best experimental conditions for nanogel preparation. This design uses the points that minimize the variance associated with the estimates of the specified model coefficients. This design is established algorithmically to present the most accurate estimates of the model equations. The best model fitting to the test data via D-optimal design was assessed by Design-Expert statistical software (version 6.1, Stat-Ease Inc., Minneapolis, USA) which was used for the generation of the experimental design matrix. This design presented a statistical model to describe the effects of preparation conditions on the nanogel size, PDI, loading efficiency and loading capacity. To fit the polynomial model to the data, a stepwise regression model was utilized. The normal probability plot and Cook's distance were applied to the detection of outliers. A lack of fit test with the ANOVA model, a plot of the residuals versus predicted values, leverage and a graphical demonstration of the experimental versus predicted values demonstrated the suitability of the model. Response surfaces plots were prepared to analyze the optimum conditions for the dependent variables.

2.3. Nanogel preparation

As the starting point, chitosan solutions with specified concentrations were prepared in sodium acetate buffer (final sodium acetate concentration of 5.54%, w/v; pH 4) under continuous mixing at 2000 rpm for 3 h. On the other hand, the ionic gelifying solution was prepared by dissolving pre-determined amounts of TPP in distilled water to obtain the desired concentrations needed according to the experimental requirements. As the typical procedure, the TPP solution was added in a drop-wise manner to the chitosan

Table 1
Experimental design and results of Plackett Burman design.

Run	Independent variables						Dependent variables	
	pH	Addition time (min)	TPP conc. % (w/v)	Temp. (°C)	Stirring rate (rpm)	Chitosan (MW)	*Z*-average (*r* nm)	Loading efficiency (%)
1	5	0	2.5	0	1000	F_1	3110.8	3.51
2	5	5	0.5	50	1000	F_1	100.8	80.45
3	4	5	2.5	0	2000	F_1	410.8	4.89
4	5	0	2.5	50	1000	F_2	847.8	3.07
5	5	5	0.5	50	2000	F_1	193.8	68.35
6	5	5	2.5	0	2000	F_2	487.3	7.92
7	4	5	2.5	50	1000	F_2	279.9	8.75
8	4	0	2.5	50	2000	F_1	107.2	5.18
9	4	0	0.5	50	2000	F_2	82.5	71.73
10	5	0	0.5	0	2000	F_2	2171.3	47.14
11	4	5	0.5	0	1000	F_2	101.4	58.10
12	4	0	0.5	0	1000	F_1	1228.0	69.88

solution with the specified concentration and addition rate at a particular temperature. Thereafter, the nanodispersion was stirred for an additional 60 min in order to cure the resulting nanoparticles. Finally, nanogels were collected via centrifuging the samples at 12,000 rpm for 15 min and re-dispersing them in distilled water.

2.4. Preparation of MTX-loaded nanogels

In order to prepare drug-loaded nanogels, MTX was dissolved in the TPP solution to obtain a final concentration of 0.75 mg/ml after mixing with an oppositely charged polymer solution during the preparation process. It should be mentioned that during the optimization procedure, various ratios of MTX/CS were evaluated to select the best one; however, this factor was not among the main factors considered in the procedure. The rest of the preparation method was carried out according to the experimental runs specified by the model. All experiments were performed in triplicate.

2.5. Surface modification of the MTX-loaded nanogels

The surfaces of the MTX-loaded nanoparticles were modified in this study for the purpose of introducing them to the BBB for brain targeting of the drug, which is the ultimate goal of the project. The coating of the nanogels was performed according to the procedure described by Kreuter et al. (2003). Briefly, after the preparation of nanoparticles, polysorbate 80 was added to the final nanodispersion to a final concentration of 1% (v/v) and the mixture was stirred at room temperature for 30 min. For confirmation of proper coating, the resulting nanogels were subjected to FT-IR spectroscopy (Nicolet, model Magna-IR spectrometer 550, USA).

2.6. In vitro characterization of surface-modified and unmodified MTX-loaded nanogels

2.6.1. Particle size, particle size distribution and surface charge

Since the size and surface zeta potential of the nanogels are the major determinants of the biofate of the carriers, the statistical central and dispersion indices of the particle sizes and zeta potentials of the optimized surface-modified and unmodified MTX-loaded nanoparticles was measured using a particle size analyzer (Malvern Instruments, model Zetasizer® 3000-HS, UK) working based on the Photon Correlation Spectroscopy (PCS) technique. Samples were diluted to appropriate concentrations with distilled/filtered water if necessary. Triplicate samples were analyzed in each case.

2.6.2. Drug loading parameters

To determine the drug loaded amount (LA), an aliquot of the final re-redispersed nanogels was destroyed via the addition of 0.15 ml/ml trichloroacetic acid (TCA, 2 N). After vortex mixing (5 min) and centrifugation (12,000 × *g* for 5 min) 20 μl of supernatant was then injected into the HPLC system. Finally, the loading parameters of the drug in nanogels were calculated as:

$$\mathrm{LE} = \left[\frac{\text{MTX loaded amount (LA)}}{\text{total MTX added during the loading procedure}}\right] \times 100$$

$$\mathrm{LC} = \left[\frac{\text{MTX loaded amount (LA)}}{\text{polymer weight} + \text{MTX loaded amount}}\right] \times 100$$

where (polymer weight + MTX loaded amount) was approximately considered as the total nanoparticle weight.

2.6.3. Nanogel morphology

The morphology and possible aggregation of the nanogels was characterized using transmission electron microscopy (TEM) (Zeiss, model EM10C, Germany) and scanning electron microscopy (SEM) (Philips, model XL30, The Netherlands). For TEM imaging, samples were fixed on the copper grids, dried at room temperature and examined using TEM without being stained. For SEM imaging, freeze-dried nanogels were placed on a stub, sputter coated with gold and evaluated at 30 kV using a 6300 field emission scanning electron microscope.

2.6.4. Nanogel chemical characterization

For chemical characterization and confirmation of proper surface modification of nanogels, Fourier transform infrared spectroscopy (FT-IR) was used (Nicolet, model Magna-IR spectrometer 550, USA). MTX-loaded hydrogel nanoparticles were freeze-dried and studied by recording FT-IR spectra at a 4 cm^{-1} resolution at ambient temperature.

2.6.5. Differential scanning calorimetry (DSC)

Approximately 10 mg of freeze-dried nanogel were precisely weighed in an aluminum pan, which was then sealed for DSC evaluation. The DSC analysis was performed using a fully automated system (Mettler-Toledo, model: DSC 823 GmbH, Switzerland) under a nitrogen atmosphere at a heating rate of 10 °C/min from 25 to 320 °C.

2.6.6. In vitro drug release

Drug release profiles of coated and uncoated nanogels were investigated while suspended in physiologically simulated medium and temperature (i.e. temperature of 37 °C and phosphate-buffered saline, PBS, with a pH of 7.4). A new assembly was designed for these studies. Briefly, our system was consisted of two Franz cells as the donor and receptor phase containers separated by a dialysis membrane (Dialysis Tubing Cellulose Membrane, D9527-100FT, size: 43 mm × 27 mm, Sigma–Aldrich, USA) with a pre-determined

surface area. The vessels were double-jacketed with 37 °C water circulating between the jacket walls throughout the study. In each experiment, 40 μg of drug-loaded nanogel, dispersed in 23 ml phosphate-buffered saline (PBS; pH of 7.4), was used as the donor phase. As the receptor phase, the same volume of PBS was added to the receptor compartment and aliquots (about 100 μl) of the release medium (i.e. receptor phase) was withdrawn at predetermined time points. The amount of MTX in the release medium was quantified using the developed HPLC method. After each measurement, the same volume of fresh PBS was put back into the receptor compartment. Control experiments using a free drug solution (20 μg in 23 ml PBS, equivalent to the net drug loaded in nanogels) as the donor phase were carried out to distinguish between drug release and drug diffusion behavior. All the drug release experiments were repeated three times.

2.7. Drug assay

The MTX concentrations in the samples throughout the study were determined by a reversed-phase high performance liquid chromatography (HPLC) method. The chromatographic system consisted of a C_{18} column (Eurosphere 100-5 C18, 150 mm × 4.6 mm, Germany) as the stationary phase and a mixture of phosphate buffer (0.01 M, pH 3.9) and acetonitrile (85:15) as the mobile phase. A pump-controller unit (Knauer, Wellchrom®, model k-1001, Berlin, Germany) and a Rheodyne injector (Rheodyne, Model 7725, USA) equipped with a 20 μl loop were used for solvent delivery (flow rate 1 ml/min) and sample injection, respectively. The analyte detection was carried out at a wavelength of 307 nm by a UV-detector (Knauer, model k-2600, Berlin, Germany). The chromatograms were analyzed using compatible software (EZChrom Elite®, Germany). A complete series of analytical method validation tests were carried out on the developed HPLC method.

3. Results and discussion

3.1. Factorial design

3.1.1. Screening

Basically, the development of an optimized method needs many experimental runs to be performed which the number of experiments increasing exponentially with an increasing number of independent variables. To decrease the number of experiments, a reduction in the number of independent variables is considered following a series of screening tests. The experimental design of the current study and the results of the Plackett Burman design are summarized in Table 1. In this section, nanogel size and drug loading efficiency were the responses considered in the model. Based on the data, the Fisher's statistical test was used for the data analysis in this section (Table 3). The model *F*-values of 8.13 for the nanogel size response and 154.73 for the drug loading efficiency response imply that the models are significant. Also, *p*-values less than 0.05 indicate models terms that are significant at the probability level of 95%. Regarding the model with nanogel size and its source of variation, the *p*-value of 0.0423 for the pH of the chitosan solution shows that it has a small but significant effect on the particle size. According to the analysis of variance procedure, the combination of the pH of the chitosan solution, the addition time of the TPP solution and temperature effects accounted for nearly 75% of the variation in the nanogel size, whereas the TPP initial concentration, rate of stirring and chitosan molecular weight did not significantly influence the particle size within the ranges tested. On the other hand, in terms of the drug loading efficiency, the *p*-value of 0.0001 for the TPP initial concentration shows that it has a very significant effect on drug loading efficiency. Considering all these results, the temperature, addition time of the TPP solution and TPP initial concentration were selected as candidates for the optimization procedure. For the pH of the chitosan solution, considering its marginal significant effect, it was ignored and set at the fixed best level to obtain smaller particle sizes in all optimization experiments (i.e. pH 4). Also, in this part of the study, to reduce the independent variables, we decided to alter the TPP concentration factor to "TPP concentration/chitosan concentration" ratio form.

3.1.2. D-optimal design

As mentioned earlier, three independent variables including the "Temperature", "Addition time of the TPP solution" and "TPP concentration/chitosan concentration", along with four response variables consisting of nanogel particle size, PDI, drug loading efficiency and drug loading capacity, were selected for the final optimization studies. D-optimal design is a utility for the optimization of mixtures when restrictions regarding the experimental design are high. Table 2 shows the design and results of the experiments carried out throughout the D-optimal design. Table 3 indicates the analysis of variance for all of the reduced models; *p*-values < 0.05 imply that these models were significant. In all cases, the lack of fit tests showed that it was not significant relative to the pure error.

3.1.2.1. Multi-objective optimization. Identification of the experimental conditions which result in the best responses is the main goal in optimization studies. However, dependent variables may sometimes be contradictory and require optimal compromises to be determined between them. To overcome this problem, in a process known as multi-objective optimization (MOO), desirability functions are used (Deming, 1991). This approach was first introduced by Derringer and Suich (1980). The Derringer's desirability, *D*, is defined as the geometric mean, weighted or otherwise, of the individual desirability functions. The expression that defines the Derringer's desirability function is:

$$D = [d_1 \times d_2 \times \cdots \times d_n]^{1/n} \quad 0 < D < 1 \tag{1}$$

where n is the number of responses in the measure and d_i is the individual desirability function of each response obtained from the transformation of the individual response of each experiment. The scale of the individual desirability function ranges between $d_i = 0$ for a completely undesired response and $d_i = 1$ for a fully desired response. For a value of "*D*" close to 1, response values are near the target values. In order to calculate the d_i for each response in the individual experiments, there are three forms of desirability functions depending on whether a particular response is to be maximized, minimized or assigned a target. In this study, two dependent variables (loading efficiency and loading capacity) should be maximized and two others (particle size and PDI) should be minimized.

To maximize the corresponding responses, the desirability was determined by the following formulae:

$$\begin{aligned} d_i &= 0 && \text{if } Y_i \le \text{Low}_i \\ d_i &= \left[\frac{(Y_i - \text{Low}_i)}{(\text{High}_i - \text{Low}_i)}\right]^{wt} && \text{if } \text{Low}_i \le Y_i \le \text{High}_i \\ d_i &= 1 && \text{if } \text{High}_i \le Y_i \end{aligned} \tag{2}$$

Table 2
Independent and dependent variables, experimental design matrix, and results of D-optimal design.

Run	Variables and their constrains							
	Independent variables			Dependent variables				ODF
	Addition time (A)	Temp. (B)	TPP/CS (C)	Particle size (*Z*-average (*r* nm))	Loading efficiency	Loading capacity	PDI	Maximize[a]
	In range[a]	In range[a]	In range[a]	Minimize[a]	Maximize[a]	Maximize[a]	Minimize[a]	
Experimental design matrix and results								
1	0.0	50.0	3.00	126.6	11.67	35.17	0.61	0.21
2	5.0	50.0	3.00	121.1	37.46	62.50	0.74	0.32
3	5.0	0.0	3.00	88.5	5.05	19.10	0.30	0.01
4	5.0	50.0	0.30	143.8	42.50	16.59	0.20	0.04
5	5.0	0.0	0.30	83.9	30.99	12.56	0.79	0.00
6	0.0	25.0	0.30	66.8	51.95	19.41	0.07	0.52
7	0.0	0.0	1.65	113.6	11.66	22.56	0.28	0.26
8	2.5	50.0	1.65	47.0	31.32	43.90	0.29	0.64
9	2.5	25.0	3.00	78.4	36.43	57.70	0.44	0.61
10	5.0	25.0	1.65	100.7	63.93	61.15	0.45	0.65
11	2.5	12.5	0.97	78.3	71.23	51.65	0.32	0.76
12	0.0	0.0	0.30	67.8	47.78	18.22	0.56	0.37
13	0.0	50.0	0.30	44.1	44.30	17.06	0.32	0.43
14	0.0	0.0	3.00	59.7	6.86	24.12	0.29	0.25
15	0.0	50.0	3.00	89.0	9.33	30.40	0.60	0.24
16	5.0	0.0	3.00	109.1	7.62	26.05	0.31	0.22
17	5.0	50.0	0.30	137.2	57.34	20.75	0.21	0.29
18	5.0	50.0	3.00	120.1	20.53	48.95	0.46	0.43

[a] Constrains.

On the other hand, to minimize the corresponding data, the desirability was determined by the following formulae:

$$d_i = 1 \quad \text{if} \quad Y_i \le \text{Low}_i$$
$$d_i = \left[\frac{(\text{High}_i - Y_i)}{(\text{High}_i - \text{Low}_i)}\right]^{wt} \quad \text{if} \quad \text{Low}_i \le Y_i \le \text{High}_i \qquad (3)$$
$$d_i = 0 \quad \text{if} \quad \text{High}_i \le Y_i$$

where "High_i" and "Low_i" represent the upper and lower tolerance limits of the response, respectively. Y_i is the response value in each experiment and the superscript "wt" represents the weight factor. When all responses have the same importance, as seen here, the "wt" is 1. The desirability functions (D) according to these equations were calculated and shown in Table 2.

The desirability functions (D) for all 18 experiments were fitted to polynomial models with no detectable outliers according to the Cook's distances (data are not shown). No transformation was

Table 3
Analysis of variance for Plackett Burman and D-optimal refined models.

	Source of variations	Sum of squares	Degree of freedom	Mean square	*F* value	Prob. > *F*	
Plackett Burman design							
Particle size (*Z*-average)	Model	7,714,503	3	2,571,501	8.13	0.0082	Significant
	pH	1,842,471	1	1,842,471	5.82	0.0423	
	Addition time	2,973,568	1	2,973,568	9.40	0.0154	
	Temperature	2,898,464	1	2,898,464	9.16	0.0164	
	Residual	2,531,129	8	316,391.1			
Loading efficiency	Model	10,940.25	1	10,940.25	154.73	<0.0001	Significant
	TPP conc.	10,940.25	1	10,940.25	154.73	<0.0001	
	Residual	707.0428	10	70.70428			
D-optimal design							
Particle size (*Z*-average)	Model	8539.82	9	948.87	1.10	0.4704	Not significant
	Residual	5169.33	6	861.56			
	Lack of fit	4228.51	3	1409.50	4.49	0.1244	Not significant
	Pure error	940.83	3	313.61			
Loading efficiency	Model	6567.88	9	729.76	5.79	0.0107	Significant
	Residual	1009.07	8	126.13			
	Lack of fit	749.65	4	187.41	2.89	0.1643	Not significant
	Pure error	259.42	4	64.85			
Loading capacity	Model	4467.48	9	496.39	8.64	0.0029	Significant
	Residual	459.37	8	57.42			
	Lack of fit	323.35	4	80.84	2.38	0.2111	Not significant
	Pure error	136.02	4	34.01			
PDI	Model	0.50	9	0.06	3.25	0.0557	Not significant
	Residual	0.14	8	0.02			
	Lack of fit	0.10	4	0.02	2.49	0.1993	Not significant
	Pure error	0.04	4	0.01			
ODF	Model	0.74	9	0.08	5.77	0.0108	Significant
	Residual	0.11	8	0.01			
	Lack of fit	0.05	4	0.01	0.91	0.5369	Not significant
	Pure error	0.06	4	0.02			

carried out. The *F*-value of the model ($F = 5.77$) indicates that the model is significant. Also, the lack of fit test revealed that it is not significant relative to the pure error. The relatively high *R*-squared (0.8665) and adjusted *R*-squared (0.7162) values implied a good relationship between the experimental data and those of the fitted models. Adequate precision was defined as a signal-to-noise ratio greater than 4; therefore, the obtained ratio of 7.676 indicates an adequate signal. The final mathematical modeling in terms of coded factors offered by the software for the nanogels preparation was developed as follows, where *A*, *B* and *C* are "addition time of the TPP solution", "temperature" and "TPP/chitosan concentration", respectively:

$$\begin{aligned}\text{Desirability function} &= 0.0822 - 0.047 \times A + 0.069 \times B \\ &- 0.003 \times C - 0.207 \times A^2 - 0.245 \times B^2 - 0.149 \times C^2 \\ &+ 0.034 \times A \times B + 0.076 \times A \times C + 0.010 \times B \times C \end{aligned} \quad (4)$$

The location of the optimum was identified to be at $A = 2.15$ min, $B = 28.05\,^{\circ}C$ and $C = 1.18$ obtained by the differentiation of the quadratic model given by Eq. (4). The predicted optimal nanogel preparation protocol corresponding to these values was 57.91, 63.04, 54.32 and 0.26 for particle size, loading efficiency, loading capacity and PDI, respectively. This condition corresponds to the maximum desirability function within the range of experimental values ($D = 0.815$). To confirm the model adequacy, five additional experiments using this optimum condition were performed. The five replicate experiments yielded an average particle size of 59.27, loading efficiency of 61.82, loading capacity of 53.68 and PDI of 0.35. The good agreement between the predicted and experimental results verifies the validity of the model and the existence of an optimal point. The response surface model graphs shown in Fig. 1 were based on the final model, holding one variable constant at its optimum level, while varying the other two within their experimental ranges. Fig. 1a presents the response surface for the optimum level of "TPP/chitosan concentration". The minimum response (desirability function) occurred when both "temperature" and "addition time" were at their lowest and highest levels, respectively. Analysis of response at the different levels of the factors revealed that there was no remarkable interaction between "temperature" and "addition time" at the optimum level of "TPP/chitosan". At the optimum level of temperature (Fig. 1b), the minimum response was seen with a low level of "TPP/chitosan" (0.3) and a high level of "addition time". Also, at different levels of "TPP/chitosan", the response varied noticeably along the axis representing the "addition time" axis. This suggests considerable interaction between these factors. Using similar reasoning regarding the response surface at the optimum level of "addition time" (Fig. 1c), it was concluded that there was a mild interaction between "TPP/chitosan" and "temperature". Also, the minimum value of the response was located at the lowest level of "temperature" and the highest level of "TPP/chitosan". The convex form of these three graphs reveals that the maximum response (i.e. desirability function) could be obtained in these ranges of the factor levels. It means that we can achieve the best conditions via this model at the about-middle points of the levels in each of the three graphs. In addition, it is clear that the amount of loading parameters exert contradictory behavior on particle size desirability; thus, considering cases such as this one, the determination of the optimum point is one of the most important parts of a nanoparticulate drug delivery study.

3.2. Nanogel preparation

Nanogels were fabricated via the ionotropic gelation procedure. This method is based on the ability of chitosan to generate a gel structure after contacting with polyanions such as TPP by forming inter- and intra-molecular linkages. The optimum combination of independent variables and their corresponding values were estimated by D-optimal experimental design. After the initial estimation, the optimal setting was validated by nanogel preparation using the specified conditions followed by the determination of particle size, PDI, loading efficiency and loading capacity in each case. As mentioned before, the optimum setting indicated earlier in the nanoparticle preparation method was reliable and highly robust with the outputs being highly consistent with the theoretical data.

3.3. Characterization of surface-modified and unmodified MTX-loaded nanogels

3.3.1. Particle size and surface potential

The final particle sizes corresponding to the optimal conditions were 59.27 ± 15.93 nm (*Z*-average (*r* nm)) for unmodified nanogels and 53.34 ± 7.23 nm (*Z*-average (*r* nm)) for surface-modified MTX-loaded nanogels. The particles obtained in the present study were unidisperse (unimodal curves) with very suitable sizes (about 100 nm), in terms of both central tendency and dispersity indices with respect to the intended intravenous route of drug delivery. Most importantly, all the mean, median and modal diameters remained without any significant changes after the surface modification procedure ($p > 0.05$). Furthermore, the size dispersity of the nanoparticle population was about the same in coated and uncoated nanogels (PDI values of 0.34 and 0.36 for uncoated and coated nanogels, respectively). This means that, under the optimum conditions, the surface modification procedure has no significant effect on particle size and the size distribution of the nanoparticles. Interestingly, the small size of MTX-loaded nanoparticles obtained in this study is a favorable prerequisite for a long circulating drug delivery system and for bypassing the BBB (Kreuter, 2001; Lu et al., 2005). The particle size is an important property that affects endocytosis by brain capillary endothelial cells. Nanoparticles less than 200 nm are more easily transported across the BBB and are less likely to be filtered by the spleen. Also, it has been reported that nanoparticles with sizes above 300 nm are easily captured by Kupffer cells or other phagocytic cells which severely limits their biodistribution. Particles below 100 nm with hydrophilic surfaces have prolonged circulation in the blood. These systems extend the duration of drug activity and also improve the targeting capabilities to specific sites (Wilson et al., 2010).

The zeta potential distribution diagrams of the uncoated as well as polysorbate 80-coated nanoparticles, both monodispersed, showed an overall positive mean zeta potential, i.e., $+21.92 \pm 0.83$ and $+16.13 \pm 1.56$ mV for unmodified and surface-modified nanogels, respectively. The surface modification process has clearly reduced the zeta potential of nanogels (p-value = 0.0004), which was expected considering the shielded nanogel surface because of the polysorbate coating. A series of studies in the literature have reported the positive final zeta potential of nanoparticles using the same preparation method (Fernández-Urrusuno, Calvo, Remuñán-López, Vila-Jato, & José Alonso, 1999; Pan et al., 2002; Wilson et al., 2010).

3.3.2. Drug loading efficiency (LE) and loading capacity (LC)

It is clear that the drug loading parameters for any carrier system should be high enough to reduce the total amount of delivery system to be used as the dosage unit. Under the optimal conditions, a loading efficiency of 61.82% and loading capacity of 53.68% were obtained. It was found that the drug loading parameters were maximal under the optimal conditions with a drug–polymer ratio of 1:1.44. This ratio was in the middle of the ratios analyzed in our study (data not shown), whereas it has been reported by many

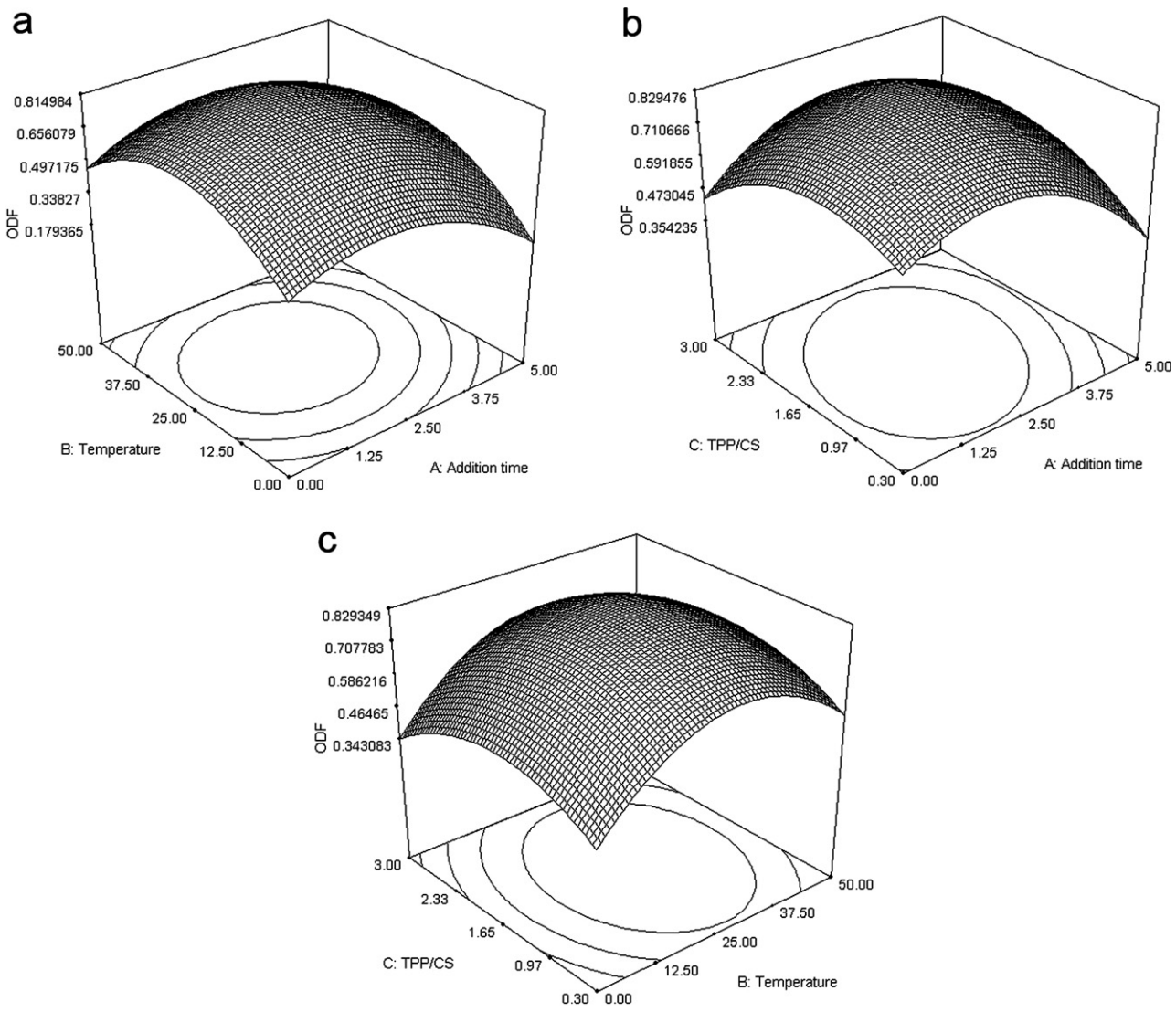

Fig. 1. Response surface of overall desirability functions: (a)–(c) fixed TPP/CS, temperature, and addition time levels at their optimum points, respectively.

authors that an increased initial drug concentration may lead to increased drug loading (Berthold, Cremer, & Kreuter, 1996; Dash, 1997; Wilson et al., 2009).

3.3.3. Nanogel morphology

Fig. 2 shows the morphological characteristics of nanoparticles obtained in our optimal setting, imaged by TEM and SEM. The size analysis of samples by TEM, while confirming the size profiles obtained by our particle size analysis, showed highly spherical shapes. In addition, the apparent hollow vacuole assembly of the nanogels as a typical behavior of the samples is noteworthy. As stated, the shapes of particles were approximately spherical and smooth in texture with an almost homogenous structure which can be attributed to the relatively gentle preparation conditions for these nanoparticles. Various studies have also reported spherical shapes (Gan & Wang, 2007), but evidence showing the formation of polyhedrons instead of spheres has also been published (Ko, Park, Hwang, Park, & Lee, 2002). However, there are no currently available reports showing the structures seen in Fig. 2a.

SEM imaging of freeze-dried nanogels (Fig. 2b) also ascertained the particulate structure of the carriers in the nanopowder form, while showing larger size dimensions, which could have occurred due to the deposition of some soluble materials on the outer surface of the nanoparticles during freeze-drying, leading to particle growth. However, redispersion of lyophilized nanogels in distilled water led to the same nano-sized particles but with somehow bigger sizes (i.e. $144.6 \pm 22.4\,d$ nm).

3.3.4. Nanogel chemical characterization

Fig. 3 shows the FT-IR spectra of chitosan (a), TPP (b), polysorbate 80 (c), uncoated chitosan-TPP nanoparticles (d) and surfactant-coated chitosan-TPP nanoparticles (e). In the chitosan spectra, the strong and broad peaks in the 3400–3200 cm^{-1} range correspond to combined peaks of O—H stretching and intermolecular hydrogen bonding. The peak at 1638 cm^{-1} in chitosan spectra (Fig. 3a) corresponds to the R—CO—NH_2 group. The peak at 1082 cm^{-1} could be attributed to stretching of the C—O group. In Fig. 3b (TPP), the regions between 900 and 1250 cm^{-1} (P=O and P—OH stretching) were selected to confirm the presence of the TPP moiety in the IR spectra of uncoated nanogels. There are several peaks in the regions between 1000 and 1250 cm^{-1} which could be related to TPP (Fig. 3d). Furthermore, two strong peaks at 1576 and 1411 cm^{-1} are related to NH_4^+ bending due to the formation of an ammonium phosphate salt. This demonstrates that interactions between the phosphate groups of the TPP molecules and the amine groups of chitosan had occurred and,

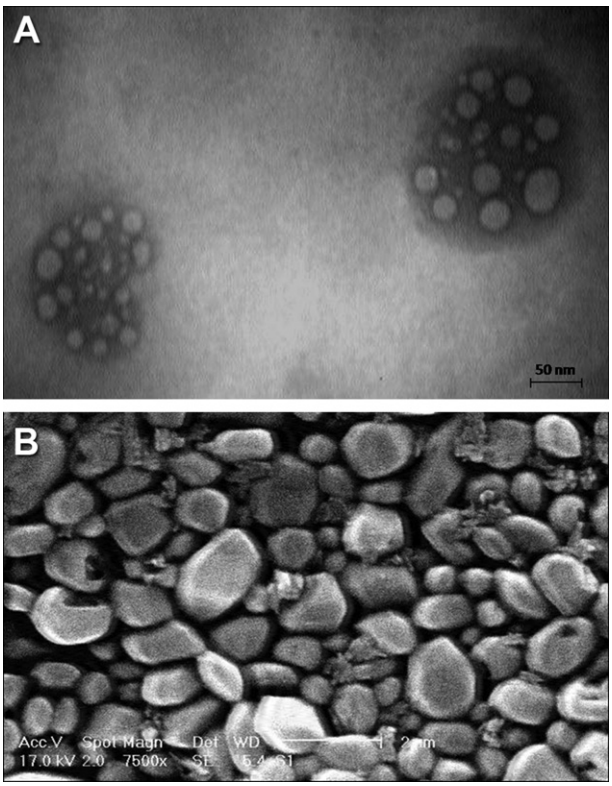

Fig. 2. TEM (a) and SEM (b) images of surface functionalized methotrexate-loaded hydrogel nanoparticles.

therefore, nanogels were formed. Comparing the FT-IR spectra before and after coating (Fig. 3d and e) revealed an enhancement in peak transmittance intensity at 2850–3000 cm^{-1} (stretching of aliphatic C—H) as it was seen in polysorbate-80 spectrum too (Fig. 3c). This was owing to the presence of polysorbate alkyl groups.

3.3.5. Differential scanning calorimetry (DSC)

Fig. 4 shows the DSC thermogram of chitosan (a), uncoated–unloaded nanogels (b), coated–unloaded nanogels (c), coated–MTX loaded nanogels (d), uncoated–MTX loaded nanogels (e), naked MTX (f) and pure TPP (g), all shown in a single graph for comparison. As shown, two definite and sharp endotherms at about 60 °C and 340 °C are evident for nanoparticles compared to chitosan and the free drug. Another endotherm, but not sharp, was recorded in about 110 °C. In fact, these three peaks are indicative of the formation of chitosan nanogels. In addition, the endotherm of the drug, methotrexate, disappeared at 160 °C in the drug-loaded nanoparticles, both coated and uncoated, and, instead, a new endotherm shoulder in 320 °C was evident for the drug-loaded nanoparticles. This observation clearly shows the involvement of some new chemical associations, e.g., new bonds between the drug and the polymer. Therefore, some "reinforcing" bonds work together with the physical drug entrapment in nanogels in the case of this drug. Third, a new exotherm at about 390–410 °C is evident for coated nanoparticles, which could be attributed to the presence of surfactant molecules on the surface of the nanoparticles, which, in turn, is supporting data showing the coating of the nanoparticles.

3.3.6. In vitro drug release

The drug release profiles from coated as well as uncoated nanogels in a dialysis setup into the surrounding buffered solution at pH 7.4 and 37 °C are shown in Fig. 5. In the control group, the free drug molecules passed through dialysis membrane and reached the equilibrium state with a lag time of about 0.5–2 h, which can probably be described by the time needed for saturation of the dialysis membrane with drug molecules. Compared with the nanogel carrier, the release rate of naked MTX was very fast, confirming the controlled drug release by the nanogels. An initial burst of release

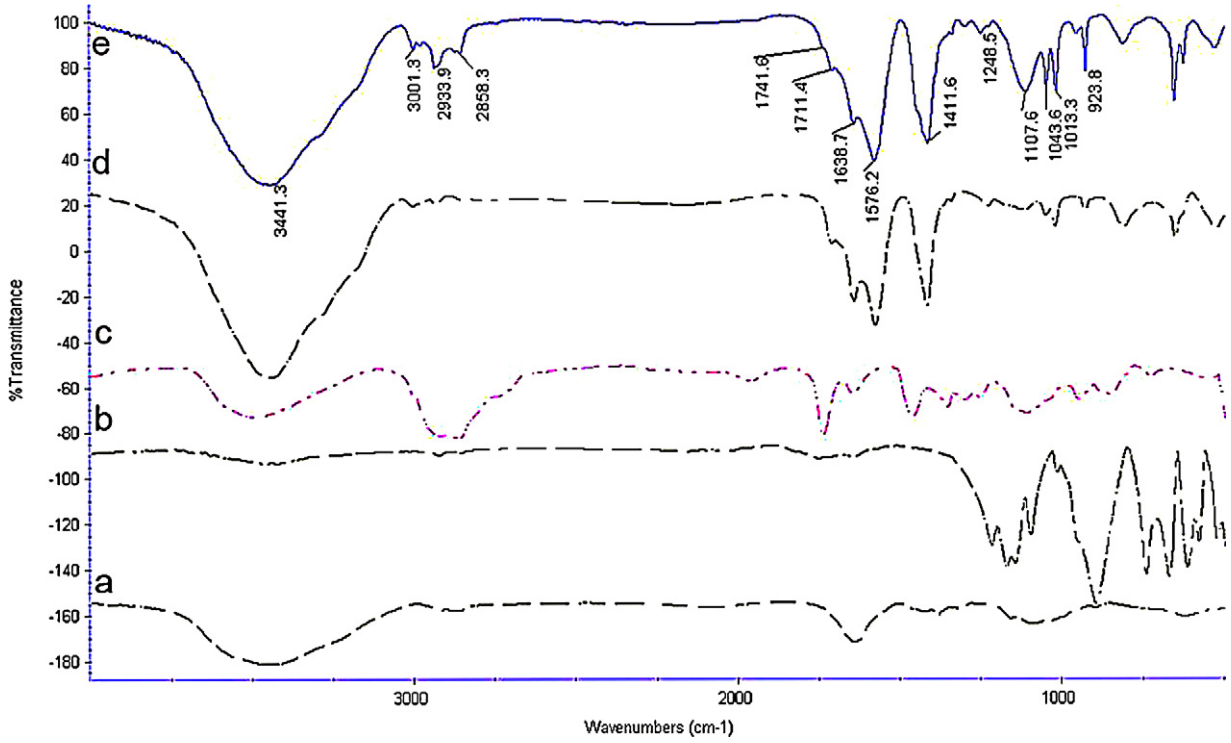

Fig. 3. FT-IR spectra of chitosan (a), TPP (b), polysorbate 80 (c), uncoated chitosan-TPP nanoparticles (d), and surfactant-coated chitosan-TPP nanoparticles (e).

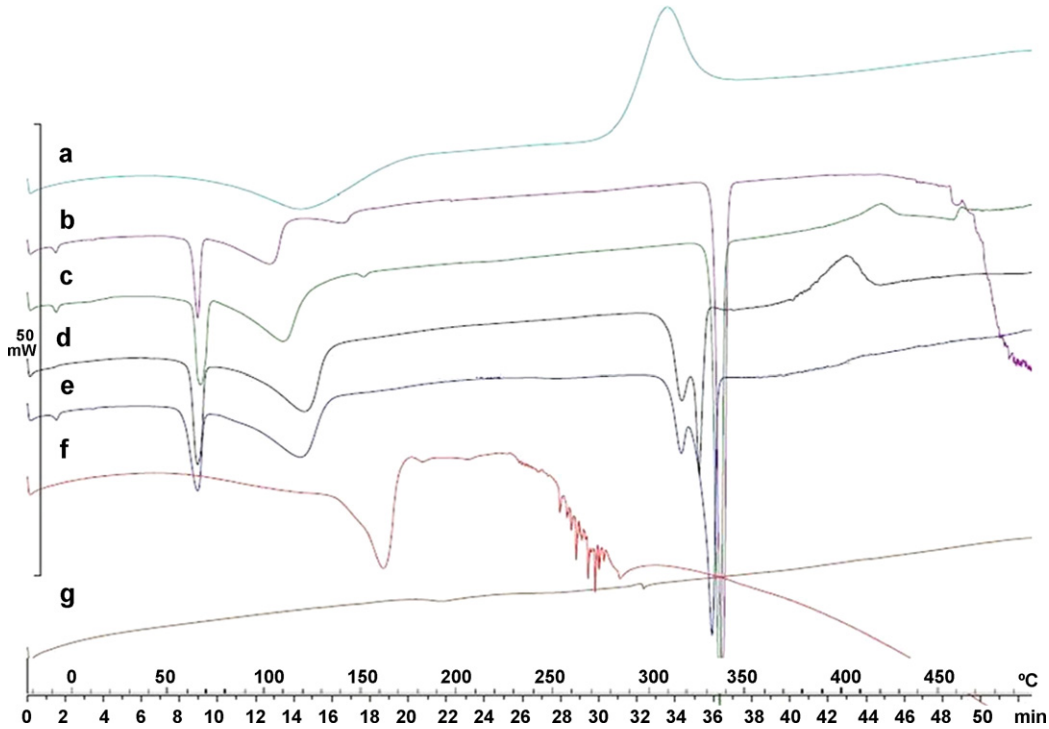

Fig. 4. Differential scanning calorimetry curves of chitosan (a), uncoated–unloaded nanogels (b), coated–unloaded nanogels (c), coated–MTX loaded nanogels (d), uncoated–MTX loaded nanogels (e), naked MTX (f), and pure TPP (g).

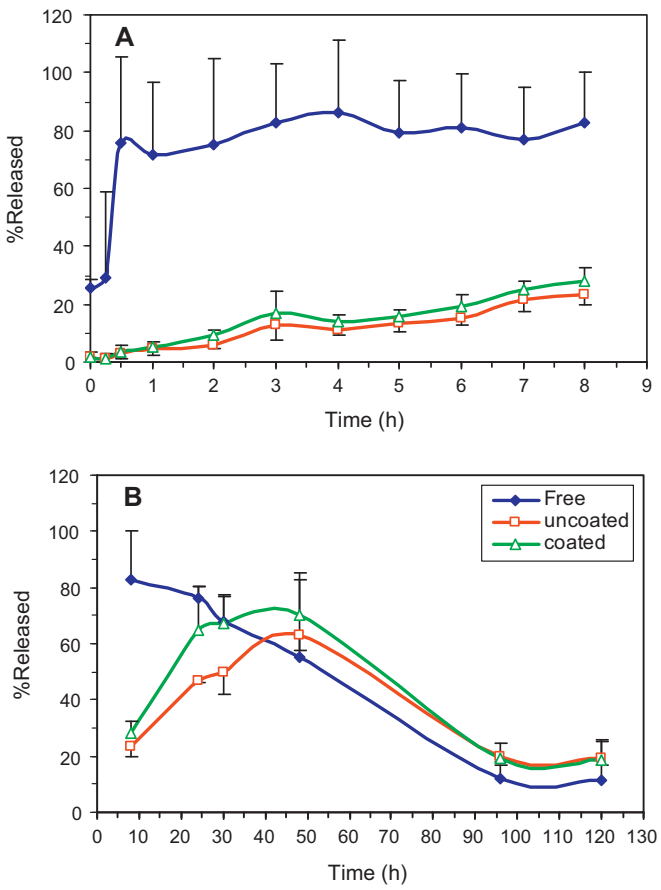

Fig. 5. The release profiles of coated nanogels, uncoated nanogels, and free drug behavior through the dialysis membrane in buffer solution with pH value of 7.4 at 37 °C (a: 0–8 h and b: 8–120 h).

was evident for both coated as well as uncoated nanogels, which can be described by the fast diffusion of the freely accessible part of the drug out of the particles, also supported by the initial particle swelling in aqueous medium. Also, a part of this burst is related to desorption of the physically adsorbed drug from the surface of nanogels. This initial burst behavior has been reported by several studies on nanogels (Janes, Fresneau, Marazuela, Fabra, & Alonso, 2001; Sarmento, Ferreira, Jorgensen, & Van De Weert, 2007; Wu, Yang, Wang, Hu, & Fu, 2005). Moreover, it is obvious that the cumulative release profiles of surfactant-coated and uncoated nanogels were almost identical. Therefore, the coating procedure itself had no discernible effect on drug release from the nanoparticles. In the case of nanogel devices such as the one we prepared in this study, the drug is uniformly dispersed/dissolved in the matrix and, thus, release occurs mainly by a combination of drug diffusion, polymer swelling and surface as well as bulk erosion of the matrix. The combination of these phenomena results in the slow drug release indicated in Fig. 5 for uncoated and surfactant-treated nanogels. This trend reached a plateau of about 65–70% release at about 48 h. Beyond this time point, a significant slowing occurred in the MTX-release profiles of coated and uncoated nanogels, which is highly consistent with the free drug release behavior, indicating that the declining trend was probably because of drug degradation under these experimental conditions. We found a mild apparent decomposition rate ($k = 0.008\ h^{-1}$) for naked MTX molecules which must be considered in future investigations.

4. Conclusion

Nanogels are potential polymeric nanoparticulate systems of interest in biomedical applications, including time-controlled drug delivery and active drug targeting. Surface functionalization of polymeric nanoparticles can play an important role in CNS distribution of these nanocarriers loaded with a drug to be delivered to the CNS. A simple and readily available preparation method was set up, optimized and validated successfully via the systematic

multi-objective optimization approach in terms of the final *Z*-average of the size, poly-dispersity index, loading efficiency and loading capacity for the fabrication of chitosan nanogels loaded with our drug of interest, methotrexate. Acceptable drug loading parameters were achieved. A series of in vitro characterization tests were carried out on the prepared nanogels with the results, collectively, confirming the suitability of the nanoparticles for our brain delivery target. The prepared nanogels were then successfully coated with polysorbate 80. The coating procedure of nanogels by the surfactant was confirmed by FT-IR. Furthermore, the surface-modified nanogels showed acceptable release performance in vitro. Considering these findings and other general excellent bio-properties of nanogels, it seems that these optimized surface-modified MTX-loaded nanogels may be a good candidate for the delivery of this anticancer agent to the CNS. In this regard, further investigations are in progress.

Acknowledgment

This study was part of a PhD thesis supported by Tehran University of Medical Sciences (TUMS); Grant no. 11852.

References

Abrey, L. E., Yahalom, J., & DeAngelis, L. M. (2000). Treatment for primary CNS lymphoma: The next step. *Journal of Clinical Oncology*, *18*, 3144–3150.

Berthold, A., Cremer, K., & Kreuter, J. (1996). Preparation and characterization of chitosan microspheres as drug carrier for prednisolone sodium phosphate as model for anti-inflammatory drugs. *Journal of Controlled Release*, *39*, 17–25.

Case, J. P. (2001). Old and new drugs used in rheumatoid arthritis: A historical perspective. Part 1. The older drugs. *American Journal of Therapeutics*, *8*, 123–143.

Dash, A. K. (1997). Determination of the physical state of drug in microcapsule and microsphere formulations. *Journal of Microencapsulation*, *14*, 101–112.

Deming, S. N. (1991). Multiple-criteria optimization. *Journal of Chromatography*, *550*, 15–25.

Derringer, G., & Suich, R. (1980). Simultaneous-optimization of several response variables. *Journal of Quality Technology*, *12*, 214–219.

Fernández-Urrusuno, R., Calvo, P., Remuñán-López, C., Vila-Jato, J. L., & José Alonso, M. (1999). Enhancement of nasal absorption of insulin using chitosan nanoparticles. *Pharmaceutical Research*, *16*, 1576–1581.

Gan, Q., & Wang, T. (2007). Chitosan nanoparticle as protein delivery carrier—systematic examination of fabrication conditions for efficient loading and release. *Colloids and Surfaces B: Biointerfaces*, *59*, 24–34.

Greig, N. H. (1992). Drug entry into the brain and its pharmacologic manipulation. *Handbook of Experimental Pharmacology*, *103*, 487–523.

Gulyaev, A. E., Gelperina, S. E., Skidan, I. N., Antropov, A. S., Kivman, G. Y., & Kreuter, J. (1999). Significant transport of doxorubicin into the brain with polysorbate 80-coated nanoparticles. *Pharmaceutical Research*, *16*, 1564–1569.

Hamidi, M., Azadi, A., Mohamadi-Samani, S., Rafiei, P., & Ashrafi, H. (2012). Valproate-loaded hydrogel nanoparticles: Preparation and characterization. *Journal of Applied Polymer Science*, *124*, 4686–4693.

Hamidi, M., Azadi, A., & Rafiei, P. (2008). Hydrogel nanoparticles in drug delivery. *Advanced Drug Delivery Reviews*, *60*, 1638–1649.

Hitchings, G. H., & Elion, G. B. (1963). Chemical suppression of the immune response. *Pharmacological Reviews*, *15*, 365–405.

Hochberg, F. H., Loeffler, J. S., & Prados, M. (1991). The therapy of primary brain lymphoma. *The Journal of Neuro-Oncology*, *10*, 191–201.

Huwyler, J., Wu, D., & Pardridge, W. M. (1996). Brain drug delivery of small molecules using immunoliposomes. *Proceedings of the National Academy of Sciences of the United States of America*, *93*, 14164–14169.

Janes, K. A., Fresneau, M. P., Marazuela, A., Fabra, A., & Alonso, M. J. (2001). Chitosan nanoparticles as delivery systems for doxorubicin. *Journal of Controlled Release*, *73*, 255–267.

Ko, J. A., Park, H. J., Hwang, S. J., Park, J. B., & Lee, J. S. (2002). Preparation and characterization of chitosan microparticles intended for controlled drug delivery. *The International Journal of Pharmaceutics*, *249*, 165–174.

Koziara, J. M., Lockman, P. R., Allen, D. D., & Mumper, R. J. (2006). The blood–brain barrier and brain drug delivery. *Journal of Nanoscience and Nanotechnology*, *9*, 2712–2735.

Kratz, F., Abu Ajaj, K., & Warnecke, A. (2007). Anticancer carrier-linked prodrugs in clinical trials. *Expert Opinion on Investigational Drugs*, *16*, 1037–1058.

Kreuter, J. (2001). Nanoparticulate systems for brain delivery of drugs. *Advanced Drug Delivery Reviews*, *47*, 65–81.

Kreuter, J., Ramge, P., Petrov, V., Hamm, S., Gelperina, S. E., Engelhardt, B., et al. (2003). Direct evidence that polysorbate-80-coated poly (butylcyanoacrylate) nanoparticles deliver drugs to the CNS via specific mechanisms requiring prior binding of drug to the nanoparticles. *Pharmaceutical Research*, *20*, 409–416.

Leiro, J., Siso, M. I. G., Ortega, M., Santamarina, M. T., & Sanmartin, M. L. (1995). A factorial experimental design for investigation of the effects of temperature, incubation time, and pathogen-to-phagocyte ration on in vivo phagocytosis by turbot adherent cells. *Comparative Biochemistry and Physiology Part C*, *112*, 215–220.

Linnet, K., & Ejsing, T. B. (2008). A review on the impact of P-glycoprotein on the penetration of drugs into the brain. Focus on psychotropic drugs. *European Neuropsychopharmacology*, *18*, 157–169.

Lu, W., Zhang, Y., Tan, Y. Z., Hu, K. L., Jiang, X. G., & Fu, S. K. (2005). Cationic albumin-conjugated pegylated nanoparticles as novel drug carrier for brain delivery. *Journal of Controlled Release*, *107*, 428–448.

Miron, J., Siso, M. I. G., Murado, M. A., & Gonzalez, M. P. (1988). Microfungus-yeast mixed cultures in the degradation of amylaceous wastes. II. An experimental design for optimization of yeast production. *Biotechnology Letters*, *2*, 171–176.

Ng, S., Rosenthal, M. A., Ashley, D., & Cher, L. (2000). High-dose methotrexate for primary CNS lymphoma in the elderly. *Neuro-Oncology*, *2*, 40–44.

Olivier, J. C., Fenart, L., Chauvet, R., Pariat, C., Cecchelli, R., & Couet, W. (1999). Indirect evidence that drug brain targeting using polysorbate 80-coated polybutylcyanoacrylate nanoparticles is related to toxicity. *Pharmaceutical Research*, *16*, 1836–1842.

Pan, Y., Li, Y., Zhao, H., Zheng, J., Xu, H., Wei, G., et al. (2002). Bioadhesive polysaccharide in protein delivery system: Chitosan nanoparticles improve the intestinal absorption of insulin in vivo. *The International Journal of Pharmaceutics*, *249*, 139–147.

Sarmento, B., Ferreira, D. C., Jorgensen, L., & Van De Weert, M. (2007). Probing insulin's secondary structure after entrapment into alginate/chitosan nanoparticles. *The European Journal of Pharmaceutics and Biopharmaceutics*, *65*, 10–17.

Stein, M., Kuten, A., Ben-Arieh, Y., Cohen, Y., & Haim, N. (1991). Primary brain lymphoma. *Harefuah*, *121*, 4–8.

Wang, Z. H., Wang, Z. Y., Sun, C. S., Wang, C. Y., Jiang, T. Y., & Wang, S. L. (2010). Trimethylated chitosan-conjugated PLGA nanoparticles for the delivery of drugs to the brain. *Biomaterials*, *31*, 908–915.

Wilson, B., Samanta, M. K., Santhi, K., Kumar, K. P., Ramasamy, M., & Suresh, B. (2010). Chitosan nanoparticles as a new delivery system for the anti-Alzheimer drug tacrine. *Nanomedicine*, *6*, 144–152.

Wilson, B., Samanta, M. K., Santhi, K., Sampath Kumar, K. P., Ramasamy, M., & Suresh, B. (2009). Significant delivery of tacrine into the brain using magnetic chitosan microparticles for treating Alzheimer's disease. *Journal of Neuroscience Methods*, *177*, 427–433.

Wong, H. L., Chattopadhyay, N., Wu, X. Y., & Bendayan, R. (2010). Nanotechnology applications for improved delivery of antiretroviral drugs to the brain. *Advanced Drug Delivery Reviews*, *62*, 503–517.

Wu, Y., Yang, W., Wang, C., Hu, J., & Fu, S. (2005). Chitosan nanoparticles as a novel delivery system for ammonium glycyrrhizinate. *The International Journal of Pharmaceutics*, *295*, 235–245.

Yuan, Q., Shah, J., Hein, S., & Misra, R. D. K. (2010). Controlled and extended drug release behavior of chitosan-based nanoparticle carrier. *Acta Biomaterialia*, *6*, 1140–1148.